Hierarchical Breakdown of RNA Structure Prediction in CASP16: From Reliable Local Features to Speculative Multimer Assembly

Chandran Nithin[1,*], Smita P Pilla[1], Sebastian Kmiecik[1,*]

[1]University of Warsaw, Biological and Chemical Research Centre, Faculty of Chemistry, Laboratory of Computational Biology, Warsaw, Poland, Zwirki i Wigury 101, 02-089 Warsaw, Poland

*To whom correspondence should be addressed: n.chandran@uw.edu.pl, sekmi@chem.uw.edu.pl

Graphical Abstract

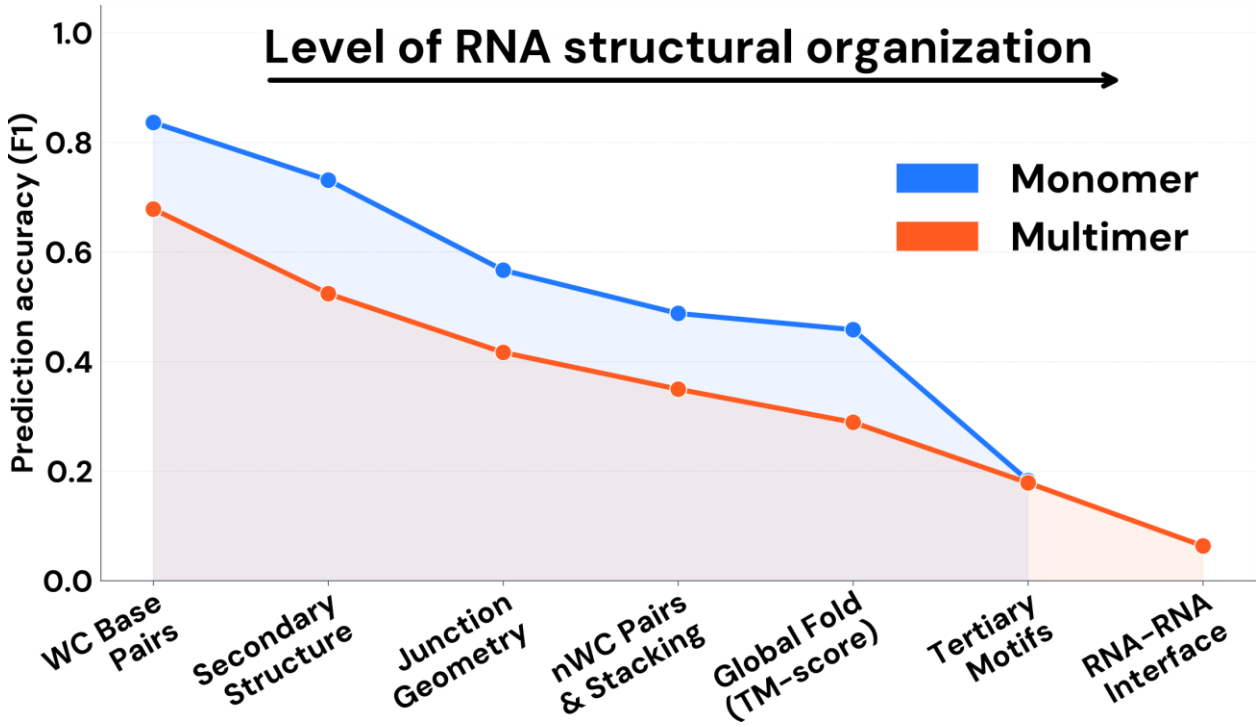

Abstract

CASP16 provided a community-wide benchmark for assessing RNA structure prediction, including the first large-scale blind assessment of RNA–RNA multimer prediction. The results showed that achieving high atomic precision remains a major challenge across the field. In this work, we use the performance of our group (LCBio) as a diagnostic case study to examine the current limits of RNA structure prediction. Our workflow ranked first in the RNA multimer category and remained competitive for monomers. We combine hierarchical analysis with representative case studies to identify a pattern of predictive breakdown, in which modeling fidelity degrades from reliable local features to increasingly speculative global architectures. Multi-helix junctions appear to mark a major transition boundary where 2D topological success often fails to translate into 3D geometric realism, leading to cascading errors in global architecture. This hierarchical breakdown is especially pronounced in RNA multimers, where limitations in the recovery of junction geometry and tertiary interactions propagate directly into errors in higher-order assembly, making multimer prediction increasingly speculative. By placing benchmark performance in a direct structural context, this case study helps define the current limits of RNA structure prediction and highlights priorities for improving predictive accuracy.

Keywords: RNA Structure prediction; CASP16; RNA modeling; RNA multimers; RNA-protein complexes

Key Points:

1. RNA structure prediction in CASP16 shows a hierarchical decline in accuracy, from relatively reliable local secondary structure to increasingly uncertain global architecture and multimer assembly.
2. Prediction accuracy declines markedly at the level of multi-helix junctions, where correct 2D topology often does not translate into realistic 3D geometry.
3. Non-canonical interactions, stacking geometry, and specialized tertiary motifs remain major sources of error in current RNA modeling pipelines.
4. High relative performance in RNA–RNA multimer prediction can be achieved despite limited atomic accuracy, highlighting the importance of expert-guided assembly and model curation.
5. Many current multimer models are better interpreted as coarse-grained organizational hypotheses than as precise atomic structures.

Introduction

The functional diversity of RNA molecules, extending from their canonical roles in the central dogma to complex regulatory and catalytic activities, is intimately linked to their ability to fold into specific three-dimensional structures (Mortimer, Kidwell, and Doudna 2014, Cao *et al.* 2024). While protein structure prediction has undergone a profound transformation driven by deep learning (Meng *et al.* 2025, Niazi 2025), de novo and ab initio prediction of RNA architecture remains fundamentally limited (Bahai *et al.* 2024, Mukherjee *et al.* 2024, Nithin *et al.* 2024, Bernard Clément *et al.* 2025, Wang J *et al.* 2025, Elofsson 2026, Ludaic and Elofsson 2026), despite recent methodological advances (Pearce, Omenn, and Zhang 2022, Justyna, Antczak, and Szachniuk 2023, Sato and Hamada 2023, Wang W *et al.* 2023, Abramson *et al.* 2024, Shen *et al.* 2024, Kagaya *et al.* 2025, Zhang S *et al.* 2026). The intrinsic flexibility of the sugar–phosphate backbone, the prevalence of non-canonical base pairing, and the strong dependence on solvent- and ion-mediated electrostatics create a vast and rugged conformational landscape that continues to test the limits of current computational methods (Justyna, Antczak, and Szachniuk 2023). As a result, RNA structure prediction remains uneven across hierarchical levels of organization, with modeling fidelity often declining from local features to global architectures.

The Critical Assessment of Protein Structure Prediction (CASP), a biennial community-wide experiment, serves as a central benchmark for evaluating and driving progress in biomolecular modeling. The recent inclusion and expansion of RNA and RNA-containing complexes as prediction targets within CASP now provide an objective framework for assessing the state of the art in RNA structure prediction (Kryshtafovych *et al.* 2023). Notably, CASP16 represented the first large-scale blind benchmark to explicitly assess RNA–RNA multimer structure prediction (Wu *et al.* 2023), introducing 11 RNA-only multimer targets alongside 35 nucleic acid monomer targets (Kryshtafovych *et al.* 2026).

Official assessment papers summarize overall performance and identify broad methodological trends (Kretsch, Albrecht *et al.* 2026, Kretsch, Hummer *et al.* 2026, Westhof *et al.* 2026). In CASP16, prediction methods fell into a limited number of broad methodological classes (Kagaya *et al.* 2026, Kong *et al.* 2026, Xiao, Shi, and Huang 2026, Zhang S *et al.* 2026)—including deep learning–based approaches, physics-informed sampling, and hybrid workflows—yet the official assessments converge on common structural limitations, particularly in modeling non-canonical interactions, multi-helix junctions, and RNA–RNA interfaces. While emerging quality assessment frameworks are beginning to provide more nuanced measures of RNA model accuracy (Bernard Clement *et al.* 2024), these community-wide evaluations necessarily abstract away the specific modeling decisions and structural failure modes encountered by individual groups.

From a participant's perspective, the practical limitations of current methods often become visible first in the specific modeling decisions—the "hand of the modeler"—including how secondary structure consensus is constructed, how homology information is interpreted, and how RNA–RNA interfaces are evaluated. This viewpoint makes it possible to connect concrete computational strategies with their structural outcomes and to pinpoint where predictive fidelity degrades from reliable local features to increasingly speculative global assemblies. In particular, it suggests that multi-helix junctions mark a major transition boundary, beyond which modeling accuracy declines and errors propagate through the structural hierarchy.

In this work, we analyze the current limits of RNA structure prediction using our group's (LCBio, G189) CASP16 results as a case study. As our pipeline achieved the top ranking in the multimer category, these models provide a useful diagnostic view of current capabilities and limitations in the field. By examining where these top-performing models succeed or fail, we show that current methods are reliable for local secondary structure but become increasingly uncertain at the level of junctions and global assembly. We therefore suggest that contemporary multimer models should often be interpreted as coarse-grained organizational hypotheses rather than precise atomic structures.

2. Methods

2.1 A Consensus-Based Pipeline for RNA Secondary Structure Prediction

RNA secondary structure prediction was performed using a consensus-based framework designed to integrate complementary sources of structural information while explicitly preserving structural uncertainty. As summarized in Figure 1 (Step 1), the pipeline combined de novo secondary structure prediction, pseudoknot-aware modeling, homology-informed refinement, and manual curation to generate secondary-structure restraints for downstream three-dimensional modeling.

For each target, an ensemble of candidate secondary structures was generated using multiple methods representing distinct methodological classes, including thermodynamic, probabilistic, and pseudoknot-aware approaches (Do, Woods, and Batzoglou 2006, Lu ZJ, Gloor, and Mathews 2009, Sato *et al.* 2009, 2011, Bellaousov and Mathews 2010, Lorenz *et al.* 2011, Ali, Mittal, and Mathews 2023). When homologous sequences or structurally related RNAs were identified, this information was used to refine the ensemble and incorporate conserved base-pairing patterns supported by external annotations or known structures (Ontiveros-Palacios *et al.* 2025, Consortium *et al.* 2026, Vallat *et al.* 2026). Additional analyses were incorporated for longer RNAs when sequence length and homolog availability made them informative (Hofacker, Priwitzer,

and Stadler 2004, Washietl and Hofacker 2004, Bernhart *et al.* 2008, Gruber *et al.* 2009, Andrews, Roche, and Moss 2018, Andrews *et al.* 2022, Zhang C, Zhang, and Pyle 2023).

All candidate structures were converted to dot-bracket notation and aggregated into a unified ensemble. Consensus base-pairing restraints were then derived from base-pair occurrence frequencies across this ensemble. To encode uncertainty explicitly, we retained two representative restraint sets for downstream three-dimensional modeling: a permissive set capturing moderately supported interactions and a stringent set retaining only universally supported base pairs. In cases of mutually exclusive pairing patterns, alternative restraint sets were preserved as separate structural hypotheses.

Following consensus construction, candidate structures were manually inspected and curated using two-dimensional representations. Manual intervention was restricted to defined stages, including adjustment of template-informed regions, alignment cleaning, inspection of consensus structures, and targeted correction of implausible base-pairing patterns. The finalized consensus structures were converted into base-pairing restraints and used as primary inputs for subsequent three-dimensional modeling. Detailed tool lists, thresholds, and target-specific decision rules are provided in Supplementary Methods S1.

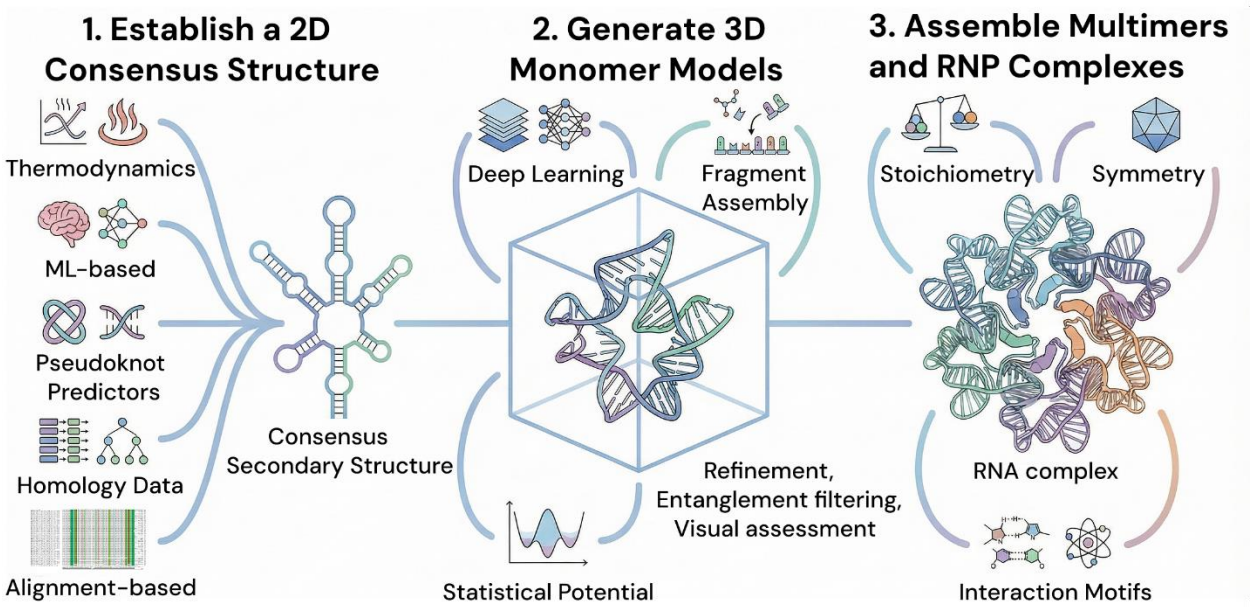

Figure 1. Three-step overview of the LCBio (189) modeling workflow used in CASP16. In Step 1, RNA secondary structure restraints are derived from a consensus of complementary prediction methods, including ViennaRNA, RNAstructure, CentroidFold, CONTRAfold, and IPknot, and are refined using homologous information from Rfam, RNAcentral, and the Protein Data Bank, with manual curation used to preserve features such as pseudoknots (Do, Woods, and Batzoglou 2006, Lu ZJ, Gloor, and Mathews 2009,

Sato *et al.* 2009, 2011, Bellaousov and Mathews 2010, Lorenz *et al.* 2011, Ali, Mittal, and Mathews 2023, Ontiveros-Palacios *et al.* 2025, Consortium *et al.* 2026, Vallat *et al.* 2026). In Step 2, candidate RNA 3D monomer models are generated using multiple complementary approaches, including DeepFoldRNA, RhoFold, BRiQ, FARFAR2, SimRNA, Vfold2, AlphaFold 3, NuFold, trRosettaNA, and RNAComposer, and are filtered and selected on the basis of structural plausibility, agreement across models, QRNAS refinement and lack of entanglements (Popenda *et al.* 2012, Boniecki *et al.* 2016, Stasiewicz *et al.* 2019, Manfredonia *et al.* 2020, Watkins Andrew Martin, Rangan, and Das 2020, Wirecki *et al.* 2020, Xiong *et al.* 2021, Li *et al.* 2022, Luwanski *et al.* 2022, Pearce, Omenn, and Zhang 2022, Wang W *et al.* 2023, Watkins Andrew M. and Das 2023, Abramson *et al.* 2024, Shen *et al.* 2024, Kagaya *et al.* 2025). In Step 3, higher-order assemblies are constructed as required, with RNA–RNA multimer modeling guided by stoichiometry, symmetry, and interface considerations, and RNA–protein complex assembly guided by structural templates and conserved interaction motifs.

2.2 A Consensus-Based Pipeline for RNA Tertiary and Complex Prediction

Consensus-derived secondary structure restraints were used as primary inputs for three-dimensional (3D) structure prediction. As outlined in Figure 1 (Steps 2 and 3), candidate monomer models were generated using multiple complementary approaches and then used as starting points for RNA–RNA multimer and RNA–protein assembly where required, through a combination of refinement, filtering, and expert-guided model selection.

To explore conformational space broadly and reduce dependence on any single modeling strategy, we generated candidate monomer models using multiple complementary approaches, including deep learning–based predictors, fragment-assembly methods, and simulation-based strategies (Popenda *et al.* 2012, Boniecki *et al.* 2016, Manfredonia *et al.* 2020, Watkins Andrew Martin, Rangan, and Das 2020, Wirecki *et al.* 2020, Xiong *et al.* 2021, Li *et al.* 2022, Pearce, Omenn, and Zhang 2022, Wang W *et al.* 2023, Watkins Andrew M. and Das 2023, Abramson *et al.* 2024, Shen *et al.* 2024, Kagaya *et al.* 2025). For methods that allowed it, modeling was performed both with and without secondary structure restraints, and models produced under different conditions were treated as independent structural hypotheses.

Across all methods, multiple candidate models were generated for each target and filtered using a combination of automated and manual criteria. Refinement was applied uniformly prior to final evaluation, and models with severe entanglements, steric clashes, self-overlap, or other physically implausible features were removed (Stasiewicz *et al.* 2019, Luwanski *et al.* 2022). Final submitted models were selected to maximize both structural plausibility and conformational diversity across the candidate pool.

For RNA–RNA multimer targets, higher-order assemblies were generated by evaluating alternative stoichiometries and arranging monomer models into candidate complexes using structural plausibility, symmetry considerations, and available template information where relevant. For RNA–protein complexes, conserved interaction motifs and homologous structural information were used to guide interface placement and assembly (Barik *et al.* 2015, Nithin, Mukherjee, and Bahadur 2019, Mukherjee and Nithin 2022). In both cases, expert-guided inspection played an important role in filtering and selecting the final submitted models.

This workflow reflects the practical modeling strategy used in CASP16: broad exploration at the monomer level, followed by increasingly selective assembly and model curation at higher levels of organization. Detailed modeling protocols, tool-specific settings, model counts, simulation parameters, and assembly procedures are provided in Supplementary Methods S2.

2.3 Official CASP16 metrics and post-CASP structural analyses

All global and interface evaluation metrics used in this study were taken directly from the official CASP16 assessment (https://predictioncenter.org/download_area/CASP16/) and were not recomputed. Composite performance measures ($Z_{monomer}$ and $Z_{multimer}$) were used to summarize overall model quality across targets. In addition to these benchmark measures, we performed feature-level analyses on the models submitted by the LCBio group in CASP16 to quantify prediction accuracy across successive levels of RNA structural organization. Structural features were extracted from both reference and predicted RNA structures using DSSR (Lu XJ, Bussemaker, and Olson 2015) to ensure consistent annotation across all models. Full definitions of structural features, scoring procedures, and aggregation rules are provided in the Supplementary Methods S3 and Supplementary Table S1.

3 Results

3.1 CASP16 performance landscape in the context of global benchmarks

The CASP16 experiment provides a comprehensive snapshot of the current state of RNA structure prediction across monomeric RNAs, RNA–RNA multimeric assemblies, and RNA–protein (RNP) complexes, evaluated using a consistent set of global accuracy metrics. As summarized in the official CASP16 assessment (Kretsch, Albrecht *et al.* 2026, Kretsch, Hummer *et al.* 2026, Westhof *et al.* 2026), RNA monomer prediction spans a broad range of quality—from near-random models to structures with recognizable overall topology—whereas RNA–RNA multimer prediction remains largely confined to a low-

accuracy regime. In contrast, RNP complexes often show a split between high-accuracy interface recovery, facilitated by structural templates, and lower-accuracy global folding.

To establish a clear reference point for the analyses that follow, Figure 2 presents the distribution of best-achieved TM-scores for each target in CASP16. This view highlights a qualitative separation between monomers and multimers that is implicit in the CASP assessment: while a substantial fraction of monomeric RNAs reach intermediate global similarity to experimental structures (exceeding the TM-score = 0.45 threshold for correct topology), RNA–RNA multimers rarely do so, even for the best-performing models. RNP complexes further demonstrate how the availability of interfacial templates can significantly boost global fold accuracy beyond that of unconstrained multimers.

This qualitative separation is not specific to CASP16 but is instead largely recapitulated across independent benchmarks. While RNA-Puzzles (Bu *et al.* 2024) and Kaggle (Lee *et al.* 2025) focus primarily on single-chain prediction, CASP16 now extends this picture to RNA–RNA multimers, showing that the fundamental limitations observed at the monomer level propagate directly into assembly.

Across these benchmarks, secondary structure and local helical geometry are frequently recovered with reasonable accuracy. In RNA-Puzzles, correct Watson–Crick pairing and stacking interactions are often predicted even when global folds are incorrect, highlighting the contrast between canonical and non-canonical interaction fidelity (Kretsch, Hummer *et al.* 2026). Similarly, as observed for CASP16 monomer targets in this work, a substantial fraction of RNAs reach an intermediate global-fold regime, while local helical elements remain comparatively reliable. All three benchmarks converge on the same practical lesson: current methods are reliable at local and secondary-structure-linked levels but lose accuracy once prediction depends on junction-mediated tertiary organization.

Importantly, refinement does not resolve these failures. Systematic benchmarking of molecular dynamics-based refinement in CASP-scale RNA datasets (Nithin, Pilla, and Kmiecik 2025) shows that MD simulations provide, at best, modest improvements for already accurate models and do not correct incorrect junction geometry or global topology. Poorly predicted models rarely benefit and often deteriorate upon refinement. These observations strengthen the interpretation that current limitations arise not simply from insufficient sampling, but from insufficient information about the higher-order structural features that determine global RNA architecture.

Within this competitive landscape, our group, LCBio (G189), demonstrated robust performance among the 64 participating groups. For RNA monomers, our submissions ranked 14th overall under the official CASP16 assessment when evaluated based on the

analysis of models with the best scores (Supplementary Figure S1A). This standing is supported by a target-by-target analysis of relative performance, which shows that our models achieved consistently above-average Z-scores across nearly all monomeric targets (Supplementary Figure S2A). Structurally, this places our monomer predictions within the intermediate-quality regime, where correct secondary structure and overall fold topology were successfully recovered for several targets.

In the RNA–RNA multimer category, our pipeline achieved its most significant result, ranking first overall among all participating groups according to the official analysis of best-scoring models (Supplementary Figure S1B). This result identifies our modeling workflow as having the highest sampling potential for RNA complexes within the CASP16 experiment. As shown in the weighted heatmap of relative performance (Supplementary Figure S2B), our models consistently outperformed the community average across both global structural metrics and interface-specific scores (e.g., ICS, IPS, and iLDDT) for almost all multimer targets. However, this relative success was achieved despite the low absolute accuracy of predicted assemblies across the field, reflecting a community-wide limitation in RNA complex modeling rather than unusually precise atomic predictions. This contrast between top-tier benchmark ranking and limited structural realism motivates the hierarchical analysis that follows.

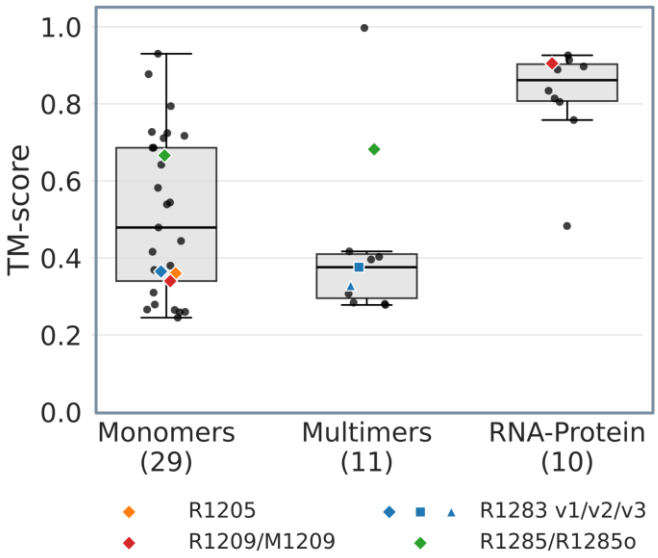

Figure 2. Overall performance of best models across all groups in CASP16 target categories. Boxplots show the distribution of TM-scores for best models across all groups in the Monomer (n = 29), RNA–RNA Multimer (n = 11), and RNA–protein complex (n = 10) categories. Individual targets are shown as grey dots. The dashed horizontal line at TM-score = 0.45 indicates a commonly used threshold for correct global topology. Case studies discussed in the text are highlighted with colored markers: R1205 (orange

diamond), R1209/M1209 (red diamond), R1283 variants (blue markers), and R1285/R1285o (green diamonds). The dual placement of the red diamonds illustrates the contrast between the incorrect RNA monomer model (R1209; TM-score < 0.45) and the RNA–protein complex model (M1209; TM-score > 0.8).

3.2 Hierarchical breakdown of predictive failure: a diagnostic deep-dive

3.2.1 Diagnostic lens and methodological framework

To identify the structural origins of the performance gap described in the previous section, we carried out a high-resolution analysis of the models submitted by the LCBio group (G189). Because this pipeline ranked first in the multimer category (Supplementary Figure S1B) while remaining competitive in the monomer category (14th overall; Supplementary Figure S1A), it offers a useful participant-level perspective on the current strengths and limitations of RNA structure prediction. Using these models as a diagnostic lens, we aimed to distinguish broad methodological success from specific structural failure modes across the organizational hierarchy (Figure 3).

The accuracy of structural features was quantified using a standardized annotation pipeline based on DSSR (Lu XJ, Bussemaker, and Olson 2015), with detailed procedures provided in Supplementary Methods S3.2. For each target, a single representative model was selected based on the highest TM-score and aligned against the corresponding experimental reference structure. Accuracy for interaction-based features was measured using the F1-score, while global fold accuracy was incorporated via the TM-score. Crucially, our evaluation employed a multi-component scoring scheme: Watson–Crick pairs were evaluated using strict matching, while non-Watson–Crick (nWC) and stacking interactions were assessed based on simultaneous agreement in base identity and geometric consistency, including orientation, distance, and interacting edges.

3.2.2 The hierarchical trend of predictive accuracy

Our analysis reveals that prediction accuracy is not lost uniformly; instead, it follows a systematic hierarchical breakdown that begins at local non-canonical elements and culminates in the failure of higher-order architecture. While global trends (Figure 3A) show that monomeric targets maintain higher accuracy than multimers, both categories exhibit a sharp decline at the transition from secondary structure to junction-mediated tertiary organization.

3.2.3 Accuracy across secondary structure and local elements

At the baseline of this hierarchy, canonical elements such as helices and stems are recovered with high fidelity (Figure 3B). However, even at this local level, a performance

gap emerges in non-canonical regions. Accuracy for internal loops, bulges, and single-stranded (SS) regions is significantly lower, particularly in multimeric targets. This is consistent with our base interaction analysis (Supplementary Figure S3), which shows that while Watson–Crick pairing is often "captured," the reliability of non-canonical interactions is markedly reduced across the entire dataset.

3.2.4 The Junction Bottleneck: topology vs. 3D geometry

Junctions represent the critical transition point where modeling reliability declines. We observe a clear "complexity wall" (Figure 3C), where accuracy for junction topology drops sharply as branching increases from three-way (3WJ) to six-way junctions (6WJ). Crucially, even when the 2D topology of a junction is correctly identified, its 3D geometry is rarely recovered (Figure 3D). While junction connectivity and linker residues show relatively high recovery, the metrics governing the spatial orientation of helices—specifically coaxial stacking—drop to near 40–50%. This inability to orient helical domains correctly around a junction core is a primary driver of global topological failure.

3.2.5 Limitations in atomic resolution and tertiary motif recovery

The breakdown continues at the level of fine-grained interactions. Decomposition of nWC base pairs (Figure 3E) and base stacking geometry (Figure 3F) shows that while base identity is often predicted, the simultaneous recovery of orientation and interacting edges (Full Match) is exceptionally rare. For nWC interactions, the failure to predict correct Leontis–Westhof edges prevents the formation of the dense interaction networks required to stabilize complex folds. Similarly, stacking interactions suffer from significant deviations in distance and angle, further destabilizing the predicted architectures. Finally, specialized tertiary motifs (Figure 3G), such as pseudoknots (PKs) and kissing loops, remain largely beyond the reach of current automated pipelines, with near-zero accuracy for several complex motif classes.

3.2.6 Error propagation and the disconnect between ranking and structural accuracy

Our analysis confirms that multimer prediction inherits and amplifies the errors of monomer modeling. This is illustrated by the discrepancy in relative performance: our pipeline achieved the top ranking in the multimer category even though the underlying monomeric subunits clustered with the main cohort of competitive groups rather than the absolute top. This disconnect between ranking and structural accuracy suggests that, at the current state of the art, multimer success depends not only on subunit quality but also on expert-guided assembly and curation. Since monomeric junctions and non-canonical interactions are rarely recovered accurately (Figure 3), multimer assembly remains partly

speculative. Consequently, many current multimer models are better interpreted as coarse-grained organizational hypotheses than as atomically accurate structures.

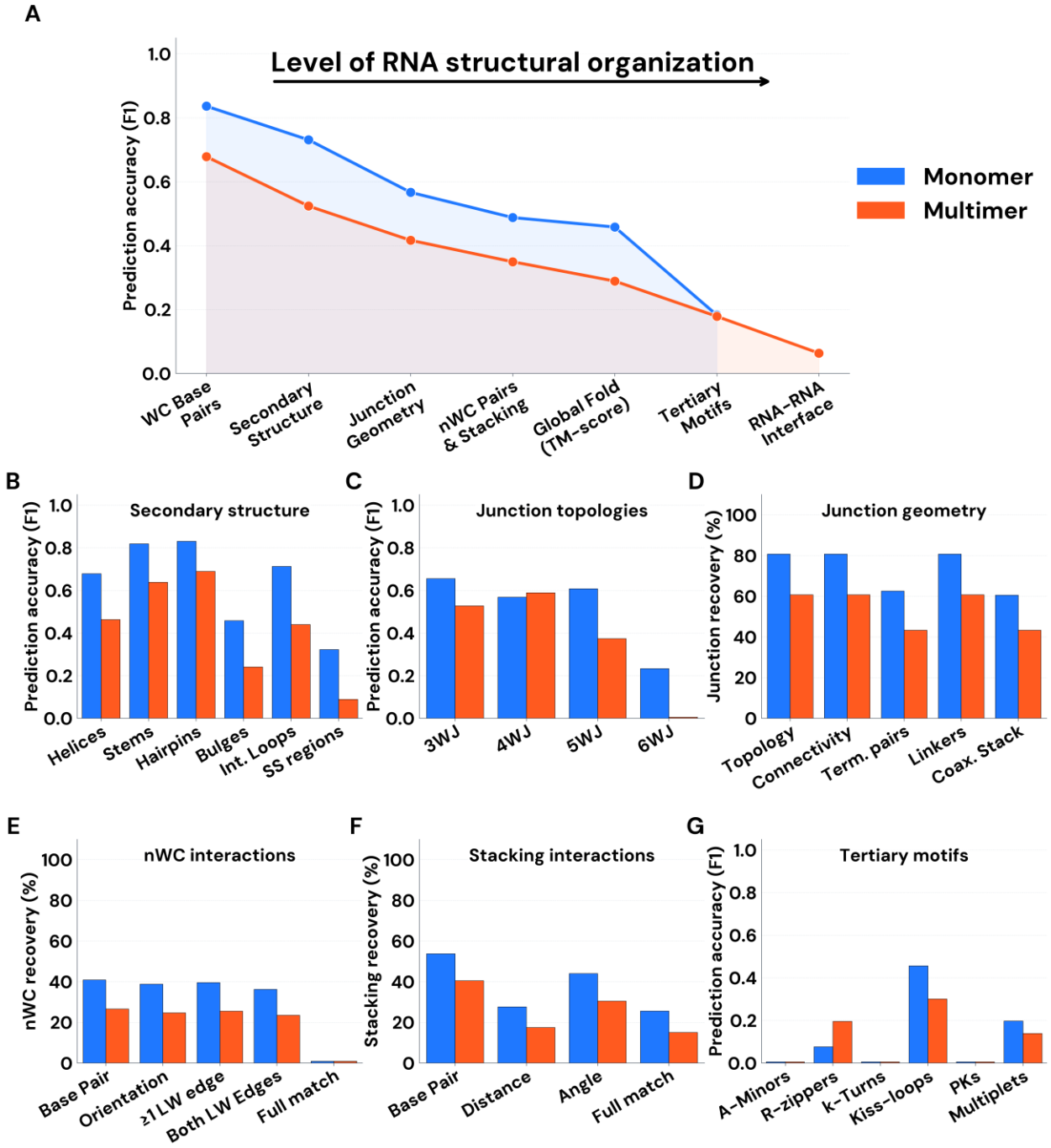

Figure 3. Hierarchical decline in RNA structure prediction accuracy. (A) Global trend of prediction accuracy (F1-score) across hierarchical levels of RNA organization, from local base pairing to global folds and multimer interfaces. (B) Accuracy for specific secondary structure elements, evaluated at the level of base pairs (helices/stems) or

residues (loops/segments). (C) Junction topology performance across increasing branching complexity (3WJ to 6WJ) and (D) recovery of junction geometry components, including connectivity and coaxial stacking. (E) Decomposition of non-Watson–Crick (nWC) base pair features and (F) stacking interaction geometry (distance and orientation) relative to reference structures. (G) Prediction accuracy for representative tertiary motifs. Results for monomeric and multimeric targets are shown in blue and orange, respectively. Detailed definitions of structural features and scoring procedures are provided in Supplementary Methods S3.2, with relative group performance heatmaps available in Supplementary Figures S1–S2.

3.3 Structural drivers of failure: representative case studies

To bridge the gap between our statistical hierarchy and concrete structural outcomes, we analyzed a set of representative targets that exemplify the "capture vs. miss" regime in current RNA modeling. These cases illustrate how the hierarchical breakdown identified in Figure 3 manifests in both monomeric and multimeric systems.

3.3.1 Architectural barriers and tertiary motifs in monomeric RNAs

The failures observed in monomeric targets R1205 and R1209 illustrate the critical transition point where modeling accuracy shifts from reliable 2D components to speculative 3D orientations.

Target R1205 (an exoribonuclease-resistant RNA; xrRNA; PDB ID: 9CFN (Gezelle *et al.* 2025)) highlights the current resolution limit of automated tertiary motif recovery. While our consensus pipeline correctly identified the 2D topology, enforcing the pseudoknot constraint during 3D modeling did not yield native-like structures (Figure 4A). Native xrRNA stabilization depends on a dense network of non-canonical base triples and specialized hairpin conformations. Consistent with the low statistical accuracy for specialized motifs across our entire dataset (Figure 3G), our models for R1205 satisfied the topological constraints at the expense of physically realistic junction geometry. This confirms that correct topology is insufficient for global structural realism when the underlying "tertiary glue"—the non-canonical interactions—is missed.

A related failure mode is seen in R1209 (HIV-1 RRE stem–loop II; PDB ID: 9C2K), which illustrates how high local fidelity can coexist with global topological failure. Here, individual helical subdomains were captured with high accuracy—a result that mirrors the broad reliability of local elements observed in our hierarchical analysis (Figure 3B). However, the global fold remained incorrect due to the misorientation of these helices at the three-way junction core (Figure 4B). This confirms that the primary architectural challenge is not the prediction of helices themselves, but the recovery of the coaxial

stacking and spatial connectivity (the components analyzed in Figure 3D) that define their relative arrangement. These cases demonstrate that junctions mark the exact boundary where modeling shifts from high-fidelity 2D capturing to speculative 3D assembly.

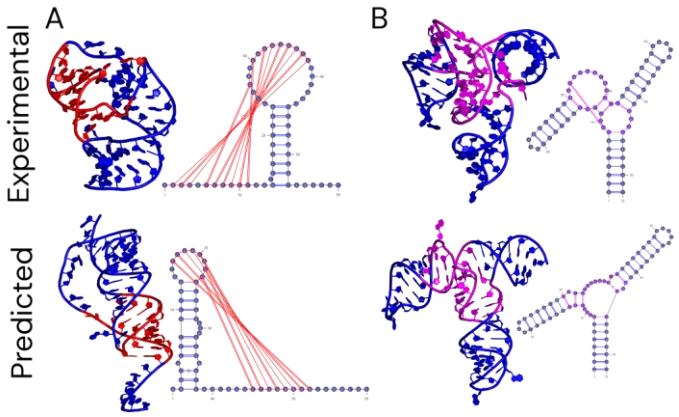

Figure 4. Errors in junction organization and tertiary contacts lead to incorrect global folds. (A) Target R1205 (xrRNA): while the correct pseudoknot topology was identified and enforced, the model failed to recover the native non-canonical base triples and specialized hairpin conformations, resulting in an incorrect global architecture. (B) Target R1209 (HIV-1 RRE stem–loop II): individual helical stems were captured with high accuracy, but incorrect coaxial stacking and helix orientation at the three-way junction core led to a misoriented, extended conformation. These examples illustrate the architectural barrier between local 2D fidelity and global 3D realism.

3.3.2 Mitigating failures through structural templates (M1209)

The prediction of target M1209 (the R1209 RNA bound to a chaperone Fab fragment; PDB ID: 9C2K) provides a vital contrast, showing how structural templates can bypass the architectural barriers that plague RNA-only modeling.

While the isolated R1209 monomer proved difficult due to its unconstrained junction, the protein–RNA complex was modeled with high accuracy (ICS and QS-scores ~0.90). By leveraging homologous structures to map the conserved "GAAACAC" RNA binding motif, we were able to precisely dock the RNA onto the Fab scaffold (Figure 5). This case demonstrates that the availability of interfacial templates can mitigate the failures seen in unconstrained systems by providing the spatial priors that automated scoring functions currently fail to provide for *de novo* folds.

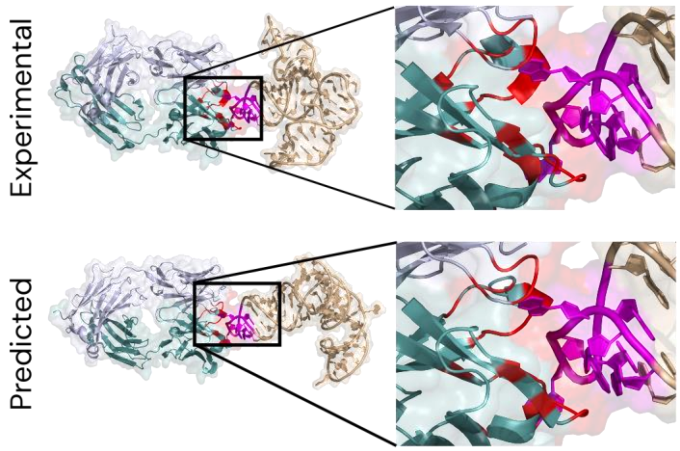

Figure 5. Accurate modeling of the RNA–protein interface in the M1209 complex. Experimental (left) and modeled (right) structures show close agreement at the protein–RNA interface (ICS and QS-scores ~0.90). The use of homologous structural templates for the Fab chaperone and the conserved GAAACAC RNA binding motif (magenta) provided sufficient spatial constraints to bypass the junctional ambiguity observed in the isolated RNA monomer (R1209), demonstrating how interfacial templates can mitigate the failures seen in unconstrained systems.

3.3.3 Coarse-grained multimer organization despite limited atomic accuracy

The RNA–RNA multimer targets R1285 and R1283 exemplify the disconnect between benchmark ranking and structural realism identified in our analysis: high competitive rankings can be achieved despite limited absolute atomic precision.

For the OLE (ornate, large, and extremophilic) RNA homodimer (R1285o; PDB ID: 9MCW (Kretsch *et al.* 2025)), our pipeline successfully identified the correct dimeric stoichiometry and approximate binding mode, securing a top ranking in CASP16. However, the top-ranked model reached a global RMSD of approximately 11 Å (**Figure 6A**). This underscores the current frontier of the field: it is possible to recover the global organizational symmetry (the "coarse-grained" hypothesis) even while failing to reproduce the realistic interaction geometry and non-canonical edges that are systematically missed across multimeric targets (Figures 3E–F).

A more complex failure occurred with R1283, a ROOL (rumen-originated, ornate, large) RNA nanostructure (Wang L *et al.* 2025). The challenge required predicting consistent architectures for monomeric (R1283v1; PDB ID: 9ISV), tetrameric (R1283v2; PDB ID: 9J3R) and octameric (R1283v3; PDB ID: 9J3T) assemblies. While individual monomeric subunits were partially consistent with the reference architecture, the pipeline failed to identify the correct multimeric assemblies, yielding only sub-assemblies (**Figure 6B**). This confirms that the systematic exploration of higher-order assembly space

remains a major challenge, as even small errors inherited from monomeric junctions propagate into large-scale shifts that preclude the formation of complex, symmetric interfaces.

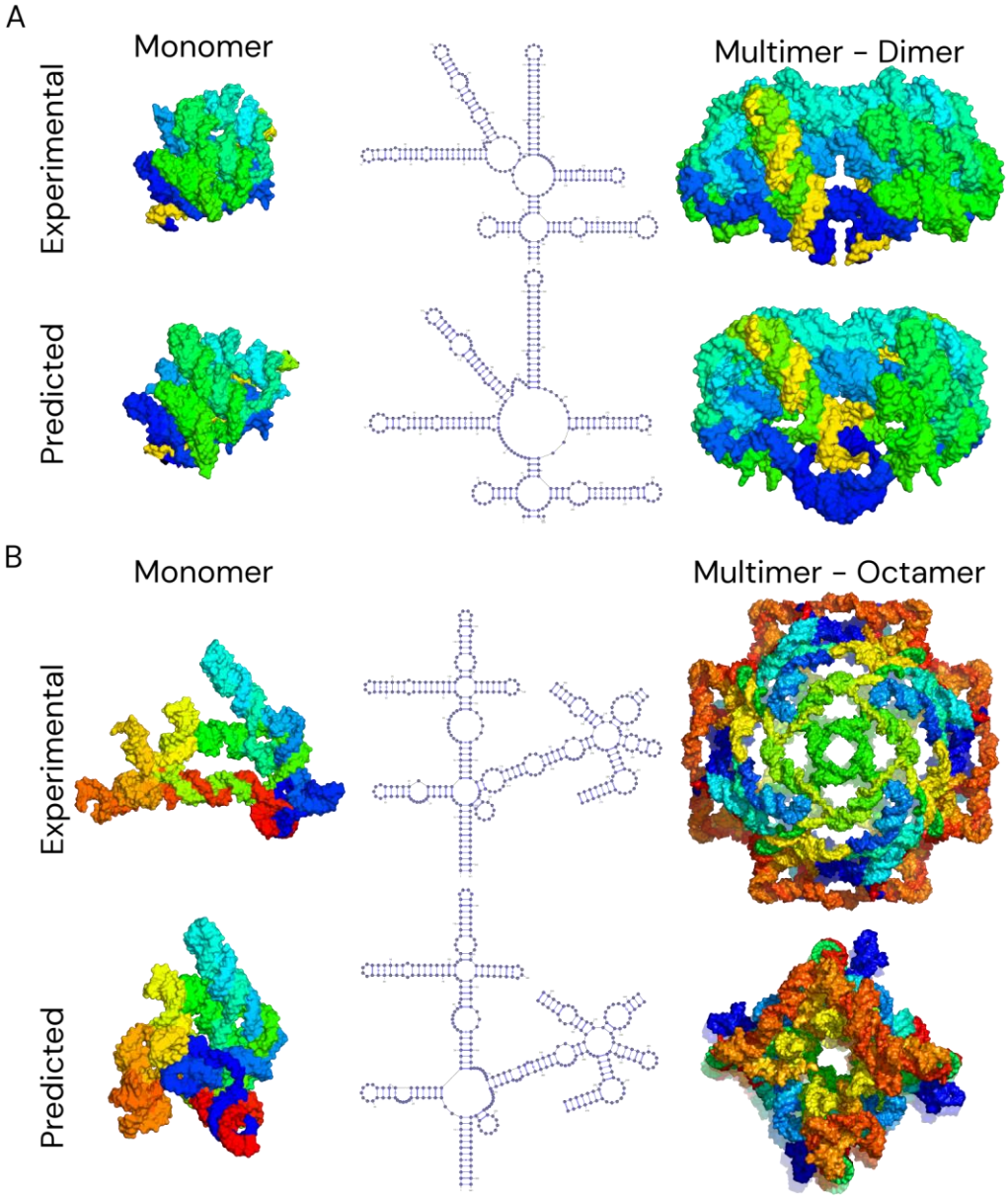

Figure 6. Coarse-grained recovery of RNA–RNA multimer assembly. (A) Target R1285 (OLE homodimer): the model correctly identified the dimeric stoichiometry and approximate arrangement of subunits, securing a top competitive ranking despite achieving low absolute atomic accuracy (global RMSD ~11 Å). **(B)** Target R1283 v1/v3 (ROOL RNA nanostructure): while the monomeric building blocks were partially consistent with the reference architecture, the modeling pipeline failed to identify the

native octameric symmetry, resulting in incomplete sub-assemblies. Secondary structure schematics are shown as VARNA diagrams.

4. Conclusions

This work provides a participant-level analysis of RNA structure prediction in CASP16, placing community-wide benchmark results in a direct structural context. By combining hierarchical performance statistics with detailed case studies, we distinguish between structural features that are currently consistently 'captured' by state-of-the-art pipelines and those that remain difficult to model in current RNA prediction workflows. Our findings illustrate that prediction accuracy is not lost at a single point but instead declines progressively across the structural hierarchy. While current methods demonstrate reliability at the level of canonical secondary structure and local helical elements, this fidelity does not consistently translate into 3D geometric realism. The transition from local elements to global architecture is strongly influenced by the spatial arrangement of helices at multi-helix junctions, which emerge as the primary source of topological errors.

The elusiveness of junctions in current modeling pipelines—stemming from their high conformational flexibility and the scarcity of reliable structural templates—means that even small angular deviations at the junction core propagate into large-scale shifts in global architecture. Recognizing this hierarchical breakdown provides a practical diagnostic for the field: it marks the point at which automated prediction shifts from high-fidelity modeling to speculative assembly. This is most clearly reflected in the performance of our modeling pipeline, which achieved a top ranking in the RNA–RNA multimer category despite a more modest standing in the monomer assessment. This discrepancy suggests that, at the current state of the art, multimer success depends both on subunit quality and on expert-guided assembly decisions.

Ultimately, the persistent failure to recover specialized tertiary motifs and accurate junction geometries across the CASP16 dataset indicates that incremental improvements in sampling or physics-based refinement are insufficient to bridge the gap to atomic realism. The fact that multimer models currently operate as coarse-grained organizational hypotheses underscores the need for better ways of representing and scoring non-canonical interaction networks. Future progress will likely require the integration of more diverse structural data into deep learning architectures and the development of scoring functions that can better capture the subtle energetic balances that govern junction-mediated tertiary organization. Addressing these cascading failures remains a central challenge for RNA structure prediction to approach the level of transformative impact currently observed in the protein folding field.

Acknowledgements

S.K., C.N., and S.P. acknowledge funding from the National Science Centre, Poland (SHENG 2021/40/Q/NZ2/00078). We gratefully acknowledge Polish high-performance computing infrastructure PLGrid (HPC Center: ACK Cyfronet AGH) for providing computer facilities and support within computational grant nos. PLG/2024/016931 and PLG/2025/017952.

Declaration of generative AI and AI-assisted technologies in the writing process

The authors employed ChatGPT (OpenAI), AI Studio (Google), Claude (Anthropic), and NotebookLM (Google) during the preparation of this manuscript to facilitate drafting and to enhance the quality of the text. The authors have reviewed and verified all AI-assisted content and take full responsibility for the final publication.

Data Availability Statement

All models submitted to CASP16 are available for download from the official CASP website at:
https://predictioncenter.org/download_area/CASP16/predictions/RNA/;
https://predictioncenter.org/download_area/CASP16/predictions/oligo/;
https://predictioncenter.org/download_area/CASP16/predictions/hybrid/.
All global and interface evaluation metrics used in this study were taken directly from the official CASP16 assessment and are available at:
https://predictioncenter.org/casp16/results.cgi?tr_type=rna;
https://predictioncenter.org/casp16/results.cgi?tr_type=rna_multi;
https://predictioncenter.org/casp16/results.cgi?tr_type=hybrid.

Conflict of Interest Statement

The authors declare that they have no competing interests.

Supplementary Materials

Supplementary Methods S1. Detailed workflow for consensus-based RNA secondary structure prediction

Supplementary Methods S2. Detailed RNA 3D modeling workflow

Supplementary Methods S3. Official CASP16 metrics and post-CASP structural analyses

Supplementary Table S1: Hierarchical feature definitions and scoring framework

Supplementary Figure S1. Official CASP16 performance rankings for the LCBio (G189) group.

Supplementary Figure S2. Weighted heatmap of relative model performance for the LCBio (G189) group across CASP16 targets.

Supplementary Figure S3. Base interaction accuracy.

5. References

Abramson J, Adler J, Dunger J *et al.* Accurate structure prediction of biomolecular interactions with AlphaFold 3. *Nature 2024 630:8016* 2024;**630**(8016):493–500. https://doi.org/10.1038/s41586-024-07487-w.

Ali SE, Mittal A, Mathews DH. RNA Secondary Structure Analysis Using RNAstructure. *Curr Protoc* 2023;**3**(7):e846. https://doi.org/10.1002/CPZ1.846.

Andrews RJ, Roche J, Moss WN. Scanfold: An approach for genome-wide discovery of local RNA structural elements-applications to Zika virus and HIV. *PeerJ* 2018;**2018**(12):e6136. https://doi.org/10.7717/PEERJ.6136/SUPP-15.

Andrews RJ, Rouse WB, O'Leary CA *et al.* ScanFold 2.0: a rapid approach for identifying potential structured RNA targets in genomes and transcriptomes. *PeerJ* 2022;**10**:e14361. https://doi.org/10.7717/PEERJ.14361.

Bahai A, Kwoh CK, Mu Y *et al.* Systematic benchmarking of deep-learning methods for tertiary RNA structure prediction. *PLoS Comput Biol* 2024;**20**(12):e1012715. https://doi.org/10.1371/JOURNAL.PCBI.1012715.

Barik A, Nithin C, Pilla SP *et al.* Molecular architecture of protein-RNA recognition sites. *J Biomol Struct Dyn* 2015;**33**(12):2738–51. https://doi.org/10.1080/07391102.2015.1004652.

Bellaousov S, Mathews DH. ProbKnot: Fast prediction of RNA secondary structure including pseudoknots. *RNA* 2010;**16**(10):1870–80. https://doi.org/10.1261/RNA.2125310.

Bernard Clement, Postic G, Ghannay S *et al.* RNAdvisor: a comprehensive benchmarking tool for the measure and prediction of RNA structural model quality. *Brief Bioinform* 2024;**25**(2). https://doi.org/10.1093/BIB/BBAE064.

Bernard Clément, Postic G, Ghannay S *et al.* Has AlphaFold3 achieved success for RNA? *Acta Crystallogr D Struct Biol* 2025;**81**(Pt 2):49–62. https://doi.org/10.1107/S2059798325000592.

Bernhart SH, Hofacker IL, Will S *et al.* RNAalifold: Improved consensus structure prediction for RNA alignments. *BMC Bioinformatics* 2008;**9**(1):474-. https://doi.org/10.1186/1471-2105-9-474.

Boniecki MJ, Lach G, Dawson WK *et al.* SimRNA: a coarse-grained method for RNA folding simulations and 3D structure prediction. *Nucleic Acids Res* 2016;**44**(7):e63–e63. https://doi.org/10.1093/NAR/GKV1479.

Bu F, Adam Y, Adamiak RW *et al.* RNA-Puzzles Round V: blind predictions of 23 RNA structures. *Nature Methods 2024 22:2* 2024;**22**(2):399–411. https://doi.org/10.1038/s41592-024-02543-9.

Cao X, Zhang Y, Ding Y *et al.* Identification of RNA structures and their roles in RNA functions. *Nature Reviews Molecular Cell Biology 2024 25:10* 2024;**25**(10):784–801. https://doi.org/10.1038/s41580-024-00748-6.

Consortium TRna, Green A, Ribas CE *et al.* RNAcentral in 2026: genes and literature integration. *Nucleic Acids Res* 2026;**54**(D1):D303–13. https://doi.org/10.1093/NAR/GKAF1329.

Do CB, Woods DA, Batzoglou S. CONTRAfold: RNA secondary structure prediction without physics-based models. *Bioinformatics* 2006;**22**(14):e90–8. https://doi.org/10.1093/BIOINFORMATICS/BTL246.

Elofsson A. AlphaFold3 at CASP16. *Proteins: Structure, Function, and Bioinformatics* 2026;**94**(1):154–66. https://doi.org/10.1002/PROT.70044.

Gezelle JG, Korn SM, McDonald JT *et al.* A conserved viral RNA fold enables nuclease resistance across kingdoms of life. *Nucleic Acids Res* 2025;**53**(16):840. https://doi.org/10.1093/NAR/GKAF840.

Gruber AR, Findeiß S, Washietl S *et al.* RNAZ 2.0: *Biocomputing 2010* Oct. 2009:69–79. https://doi.org/10.1142/9789814295291_0009.

Hofacker IL, Priwitzer B, Stadler PF. Prediction of locally stable RNA secondary structures for genome-wide surveys. *Bioinformatics* 2004;**20**(2):186–90. https://doi.org/10.1093/BIOINFORMATICS/BTG388.

Justyna M, Antczak M, Szachniuk M. Machine learning for RNA 2D structure prediction benchmarked on experimental data. *Brief Bioinform* 2023;**24**(3):1–9. https://doi.org/10.1093/BIB/BBAD153.

Kagaya Y, Nakamura T, Verburgt J *et al.* Structure Modeling Protocols for Protein Multimer and RNA in CASP16 With Enhanced MSAs, Model Ranking, and Deep Learning. *Proteins: Structure, Function, and Bioinformatics* 2026;**94**(1):167–82. https://doi.org/10.1002/PROT.70033.

Kagaya Y, Zhang Z, Ibtehaz N *et al.* NuFold: end-to-end approach for RNA tertiary structure prediction with flexible nucleobase center representation. *Nature Communications 2025 16:1* 2025;**16**(1):881-. https://doi.org/10.1038/s41467-025-56261-7.

Kong R, Jiang Z, Lu X *et al.* Ligand Binding Prediction on Pharmaceutical and Nucleic Acid Targets by the CoDock Group in CASP16. *Proteins: Structure, Function, and Bioinformatics* 2026;**94**(1):276–85. https://doi.org/10.1002/PROT.70032.

Kretsch RC, Albrecht R, Andersen ES *et al.* Functional Relevance of CASP16 Nucleic Acid Predictions as Evaluated by Structure Providers. *Proteins: Structure, Function, and Bioinformatics* 2026;**94**(1):51–78. https://doi.org/10.1002/PROT.70043.

Kretsch RC, Hummer AM, He S *et al.* Assessment of Nucleic Acid Structure Prediction in CASP16. *Proteins: Structure, Function, and Bioinformatics* 2026;**94**(1):192–217. https://doi.org/10.1002/PROT.70072.

Kretsch RC, Wu Y, Shabalina SA *et al.* Naturally ornate RNA-only complexes revealed by cryo-EM. *Nature 2025 643:8073* 2025;**643**(8073):1135–42. https://doi.org/10.1038/s41586-025-09073-0.

Kryshtafovych A, Milostan M, Lensink MF *et al.* Updates to the CASP Infrastructure in 2024. *Proteins: Structure, Function, and Bioinformatics* 2026;**94**(1):15–24. https://doi.org/10.1002/PROT.70042.

Kryshtafovych A, Schwede T, Topf M *et al.* Critical assessment of methods of protein structure prediction (CASP)—Round XV. *Proteins: Structure, Function, and Bioinformatics* 2023;**91**(12):1539–49. https://doi.org/10.1002/PROT.26617.

Lee Y, He S, Oda T *et al.* Template-based RNA structure prediction advanced through a blind code competition. *BioRxiv* 30 Dec. 2025:2025.12.30.696949. https://doi.org/10.64898/2025.12.30.696949.

Li J, Zhang S, Zhang D *et al.* Vfold-Pipeline: a web server for RNA 3D structure prediction from sequences. *Bioinformatics* 2022;**38**(16):4042–3. https://doi.org/10.1093/BIOINFORMATICS/BTAC426.

Lorenz R, Bernhart SH, Höner zu Siederdissen C *et al.* ViennaRNA Package 2.0. *Algorithms for Molecular Biology* 2011;**6**(1):26-. https://doi.org/10.1186/1748-7188-6-26.

Lu XJ, Bussemaker HJ, Olson WK. DSSR: an integrated software tool for dissecting the spatial structure of RNA. *Nucleic Acids Res* 2015;**43**(21):e142–e142. https://doi.org/10.1093/NAR/GKV716.

Lu ZJ, Gloor JW, Mathews DH. Improved RNA secondary structure prediction by maximizing expected pair accuracy. *RNA* 2009;**15**(10):1805–13. https://doi.org/10.1261/RNA.1643609.

Ludaic M, Elofsson A. Limits of deep-learning-based RNA prediction methods. *BioRxiv* 13 Mar. 2026:2025.04.30.651414. https://doi.org/10.1101/2025.04.30.651414.

Luwanski K, Hlushchenko V, Popenda M *et al.* RNAspider: a webserver to analyze entanglements in RNA 3D structures. *Nucleic Acids Res* 2022;**50**(W1):W663–9. https://doi.org/10.1093/NAR/GKAC218.

Manfredonia I, Nithin C, Ponce-Salvatierra A *et al.* Genome-wide mapping of SARS-CoV-2 RNA structures identifies therapeutically-relevant elements. *Nucleic Acids Res* 2020;**48**(22):12436–52. https://doi.org/10.1093/NAR/GKAA1053.

Meng Y, Zhang Z, Zhou C *et al.* Protein structure prediction via deep learning: an in-depth review. *Front Pharmacol* 2025;**16**:1498662. https://doi.org/10.3389/FPHAR.2025.1498662/XML.

Mortimer SA, Kidwell MA, Doudna JA. Insights into RNA structure and function from genome-wide studies. *Nature Reviews Genetics 2014 15:7* 2014;**15**(7):469–79. https://doi.org/10.1038/nrg3681.

Mukherjee S, Moafinejad SN, Badepally NG *et al.* Advances in the field of RNA 3D structure prediction and modeling, with purely theoretical approaches, and with the use of experimental data. *Structure* 2024;**32**(11):1860–76. https://doi.org/10.1016/J.STR.2024.08.015.

Mukherjee S, Nithin C. Advanced computational tools for quantitative analysis of protein–nucleic acid interfaces. *Advances in Protein Molecular and Structural Biology Methods* 1 Jan. 2022:163–80. https://doi.org/10.1016/B978-0-323-90264-9.00011-8.

Niazi SK. Critical assessment of AI-based protein structure prediction: Fundamental challenges and future directions in drug discovery. *Computational and Structural Biotechnology Reports* 2025;**2**:100064. https://doi.org/10.1016/J.CSBR.2025.100064.

Nithin C, Kmiecik S, Błaszczyk R *et al.* Comparative analysis of RNA 3D structure prediction methods: towards enhanced modeling of RNA–ligand interactions. *Nucleic Acids Res* 2024;**52**(13):7465–86. https://doi.org/10.1093/NAR/GKAE541.

Nithin C, Mukherjee S, Bahadur RP. A structure-based model for the prediction of protein-RNA binding affinity. *RNA* 2019;**25**(12):1628–45. https://doi.org/10.1261/RNA.071779.119.

Nithin C, Pilla SP, Kmiecik S. When does molecular dynamics improve RNA models? Insights from CASP15 and practical guidelines. *Comput Struct Biotechnol J* 2025;**27**:4201–11. https://doi.org/10.1016/J.CSBJ.2025.10.003.

Ontiveros-Palacios N, Cooke E, Nawrocki EP *et al.* Rfam 15: RNA families database in 2025. *Nucleic Acids Res* 2025;**53**(D1):D258–67. https://doi.org/10.1093/NAR/GKAE1023.

Pearce R, Omenn GS, Zhang Y. De Novo RNA Tertiary Structure Prediction at Atomic Resolution Using Geometric Potentials from Deep Learning. *BioRxiv* 15 May 2022:2022.05.15.491755. https://doi.org/10.1101/2022.05.15.491755.

Popenda M, Szachniuk M, Antczak M *et al.* Automated 3D structure composition for large RNAs. *Nucleic Acids Res* 2012;**40**(14):e112–e112. https://doi.org/10.1093/NAR/GKS339.

Sato K, Hamada M. Recent trends in RNA informatics: a review of machine learning and deep learning for RNA secondary structure prediction and RNA drug discovery. *Brief Bioinform* 2023;**24**(4):1–13. https://doi.org/10.1093/BIB/BBAD186.

Sato K, Hamada M, Asai K *et al.* CentroidFold: a web server for RNA secondary structure prediction. *Nucleic Acids Res* 2009;**37**(suppl_2):W277–80. https://doi.org/10.1093/NAR/GKP367.

Sato K, Kato Y, Hamada M *et al.* IPknot: fast and accurate prediction of RNA secondary structures with pseudoknots using integer programming. *Bioinformatics* 2011;**27**(13):i85–93. https://doi.org/10.1093/BIOINFORMATICS/BTR215.

Shen T, Hu Z, Sun S *et al.* Accurate RNA 3D structure prediction using a language model-based deep learning approach. *Nature Methods 2024 21:12* 2024;**21**(12):2287–98. https://doi.org/10.1038/s41592-024-02487-0.

Stasiewicz J, Mukherjee S, Nithin C *et al.* QRNAS: Software tool for refinement of nucleic acid structures. *BMC Struct Biol* 2019;**19**(1):5-. https://doi.org/10.1186/S12900-019-0103-1.

Vallat B, Rose Y, Piehl DW *et al.* RCSB Protein Data Bank: Delivering integrative structures alongside experimental structures and computed structure models. *Nucleic Acids Res* 2026;**54**(D1):D489–98. https://doi.org/10.1093/NAR/GKAF1187.

Wang J, Fan Y, Hong L *et al.* Deep learning for RNA structure prediction. *Curr Opin Struct Biol* 2025;**91**:102991. https://doi.org/10.1016/J.SBI.2025.102991.

Wang L, Xie J, Gong T *et al.* Cryo-EM reveals mechanisms of natural RNA multivalency. *Science (1979)* 2025;**388**(6746):545–50. https://doi.org/10.1126/SCIENCE.ADV3451.

Wang W, Feng C, Han R *et al.* trRosettaRNA: automated prediction of RNA 3D structure with transformer network. *Nature Communications 2023 14:1* 2023;**14**(1):7266-. https://doi.org/10.1038/s41467-023-42528-4.

Washietl S, Hofacker IL. Consensus Folding of Aligned Sequences as a New Measure for the Detection of Functional RNAs by Comparative Genomics. *J Mol Biol* 2004;**342**(1):19–30. https://doi.org/10.1016/J.JMB.2004.07.018.

Watkins Andrew M., Das R. RNA 3D Modeling with FARFAR2, Online. *Methods Mol Biol* 2023;**2586**:233–49. https://doi.org/10.1007/978-1-0716-2768-6_14.

Watkins Andrew Martin, Rangan R, Das R. FARFAR2: Improved De Novo Rosetta Prediction of Complex Global RNA Folds. *Structure* 2020;**28**(8):963-976.e6. https://doi.org/10.1016/J.STR.2020.05.011.

Westhof E, Sun H, Bu F *et al.* The RNA-Puzzles Assessments of RNA-Only Targets in CASP16. *Proteins: Structure, Function, and Bioinformatics* 2026;**94**(1):218–29. https://doi.org/10.1002/PROT.70052.

Wirecki TK, Nithin C, Mukherjee S *et al.* Modeling of Three-Dimensional RNA Structures Using SimRNA. *Methods in Molecular Biology* 2020;**2165**:103–25. https://doi.org/10.1007/978-1-0716-0708-4_6.

Wu KE, Zou JY, Chang H *et al.* Machine learning modeling of RNA structures: methods, challenges and future perspectives. *Brief Bioinform* 2023;**24**(4):1–12. https://doi.org/10.1093/BIB/BBAD210.

Xiao B, Shi Y, Huang L. Enhancing RNA 3D Structure Prediction: A Hybrid Approach Combining Expert Knowledge and Computational Tools in CASP16. *Proteins: Structure, Function, and Bioinformatics* 2026;**94**(1):230–8. https://doi.org/10.1002/PROT.70034.

Xiong P, Wu R, Zhan J *et al.* Pairing a high-resolution statistical potential with a nucleobase-centric sampling algorithm for improving RNA model refinement. *Nature Communications 2021 12:1* 2021;**12**(1):2777-. https://doi.org/10.1038/s41467-021-23100-4.

Zhang C, Zhang Y, Pyle AM. rMSA: A Sequence Search and Alignment Algorithm to Improve RNA Structure Modeling. *J Mol Biol* 2023;**435**(14):167904. https://doi.org/10.1016/J.JMB.2022.167904.

Zhang S, Li J, Zhou Y *et al.* Enhancing RNA 3D Structure Prediction in CASP16: Integrating Physics-Based Modeling With Machine Learning for Improved Predictions. *Proteins: Structure, Function, and Bioinformatics* 2026;**94**(1):239–48. https://doi.org/10.1002/PROT.26856.

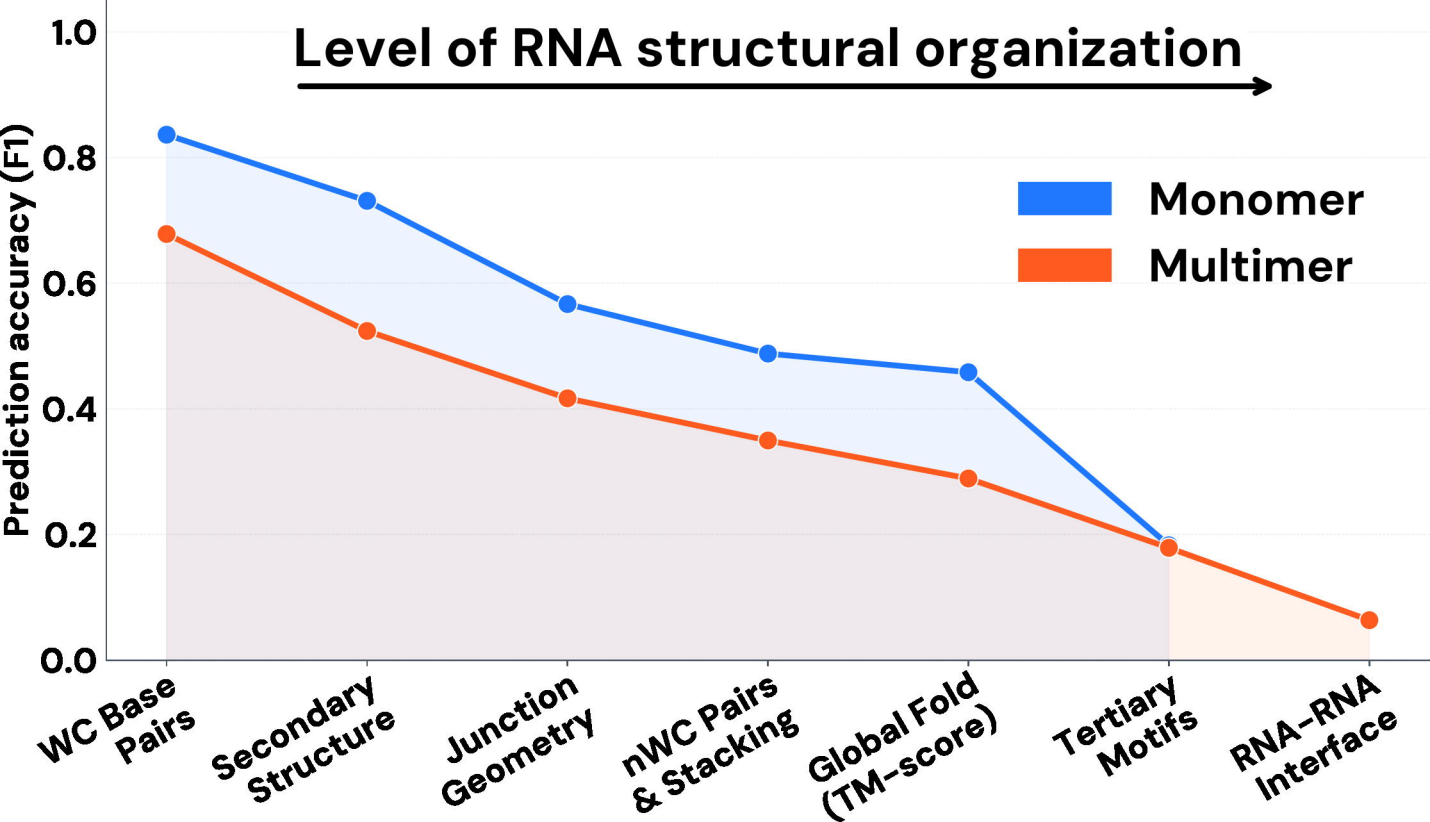
Level of RNA structural organization
Prediction accuracy (F1)
1.0
0.8
0.6
0.4
0.2
0.0
Monomer
Multimer
WC Base Pairs
Secondary Structure
Junction Geometry
nWC Pairs & Stacking
Global Fold (TM-score)
Tertiary Motifs
RNA-RNA Interface

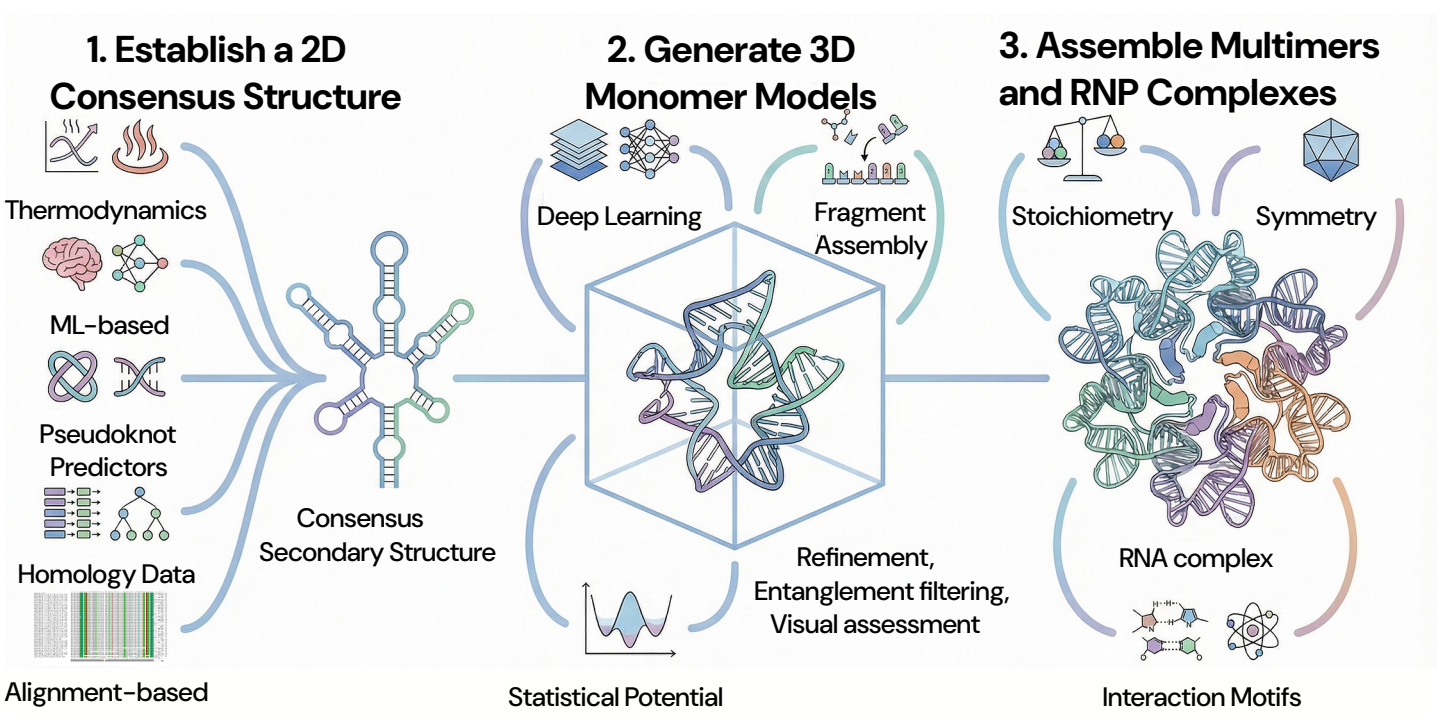
1. Establish a 2D Consensus Structure
Thermodynamics
ML-based
Pseudoknot Predictors
Homology Data
Alignment-based
Consensus Secondary Structure
2. Generate 3D Monomer Models
Deep Learning
Fragment Assembly
Refinement, Entanglement filtering, Visual assessment
Statistical Potential
3. Assemble Multimers and RNP Complexes
Stoichiometry
Symmetry
RNA complex
Interaction Motifs

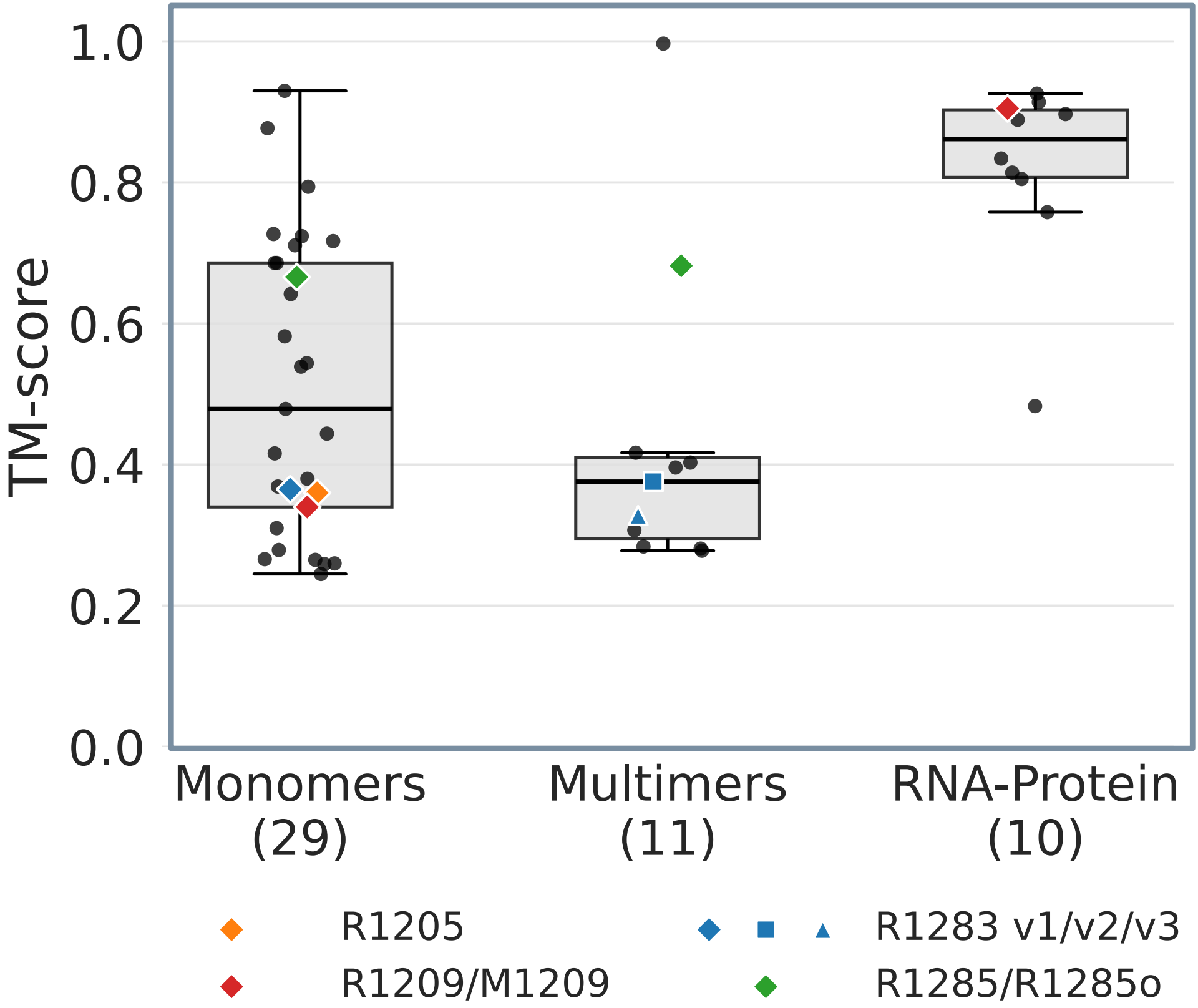
TM-score
1.0
0.8
0.6
0.4
0.2
0.0
Monomers
(29)
Multimers
(11)
RNA-Protein
(10)
R1205
R1209/M1209
R1283 v1/v2/v3
R1285/R1285o

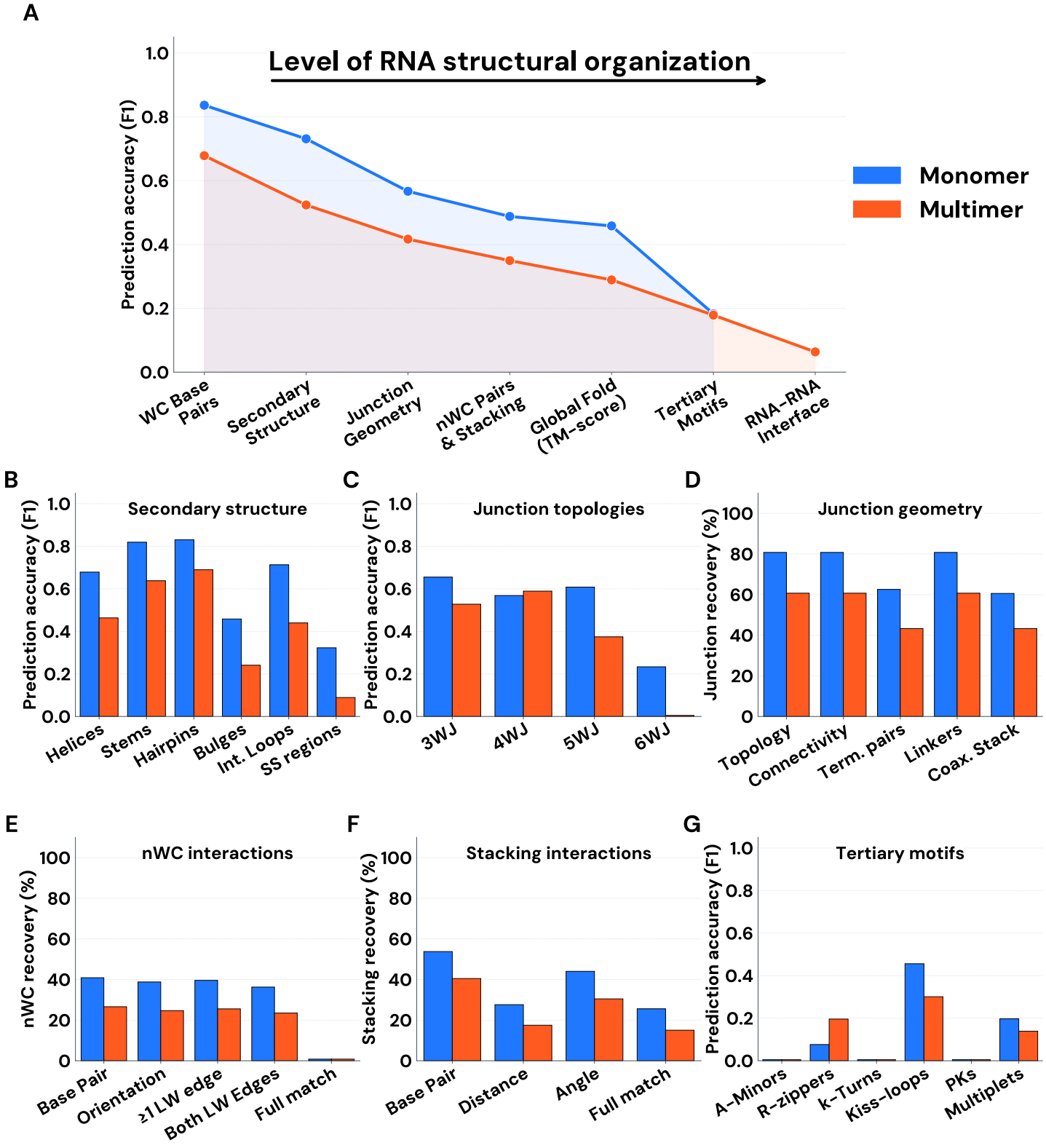
A
Level of RNA structural organization
Prediction accuracy (F1)
1.0
0.8
0.6
0.4
0.2
0.0
WC Base Pairs
Secondary Structure
Junction Geometry
nWC Pairs & Stacking
Global Fold (TM-score)
Tertiary Motifs
RNA-RNA Interface
Monomer
Multimer
B
Secondary structure
Prediction accuracy (F1)
Helices
Stems
Hairpins
Bulges
Int. Loops
SS regions
C
Junction topologies
Prediction accuracy (F1)
3WJ
4WJ
5WJ
6WJ
D
Junction geometry
Junction recovery (%)
100
80
60
40
20
0
Topology
Connectivity
Term. pairs
Linkers
Coax. Stack
E
nWC interactions
nWC recovery (%)
Base Pair
Orientation
≥1 LW edge
Both LW Edges
Full match
F
Stacking interactions
Stacking recovery (%)
Base Pair
Distance
Angle
Full match
G
Tertiary motifs
Prediction accuracy (F1)
A-Minors
R-zippers
k-Turns
Kiss-loops
PKs
Multiplets

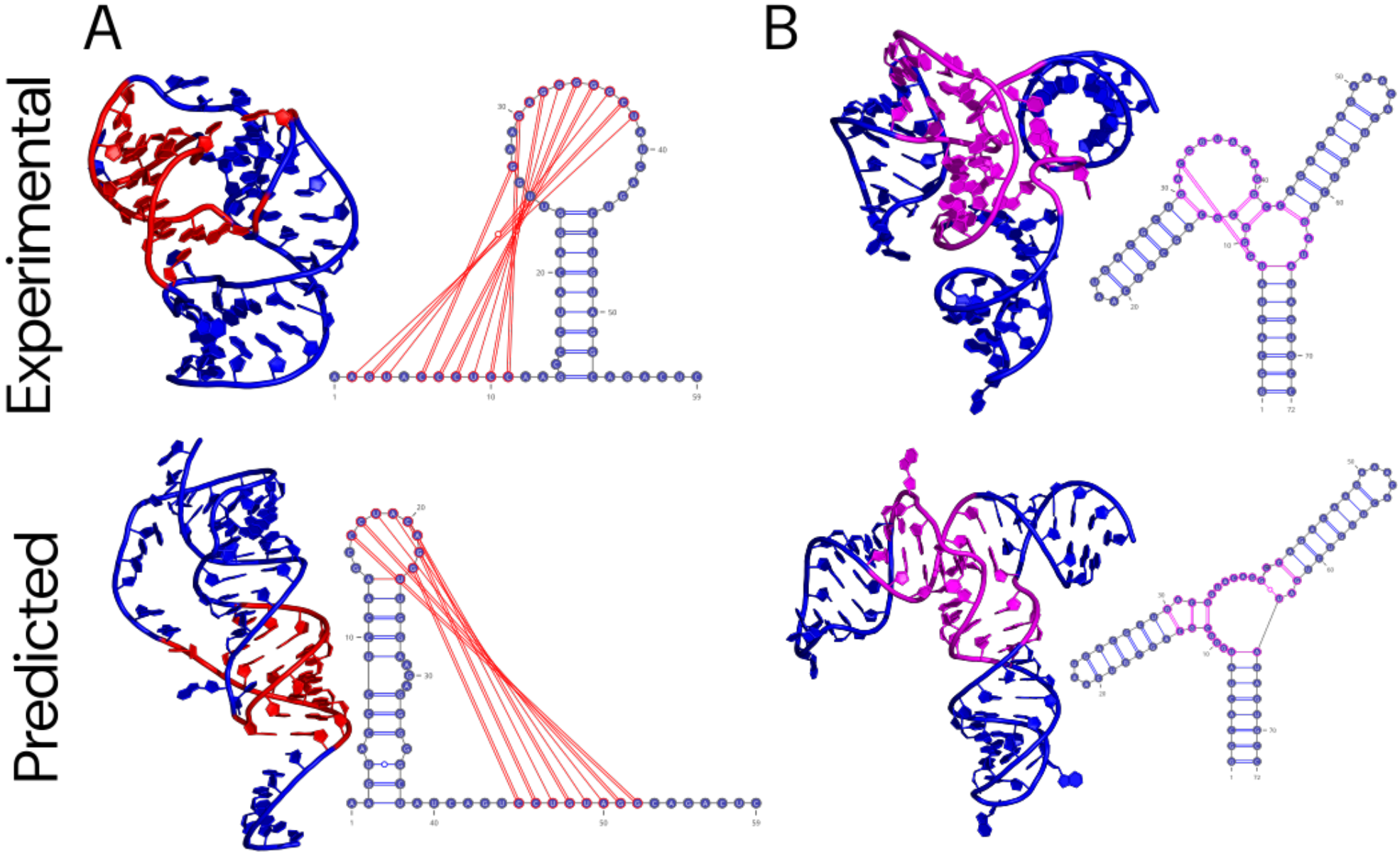
A
B
Experimental
Predicted

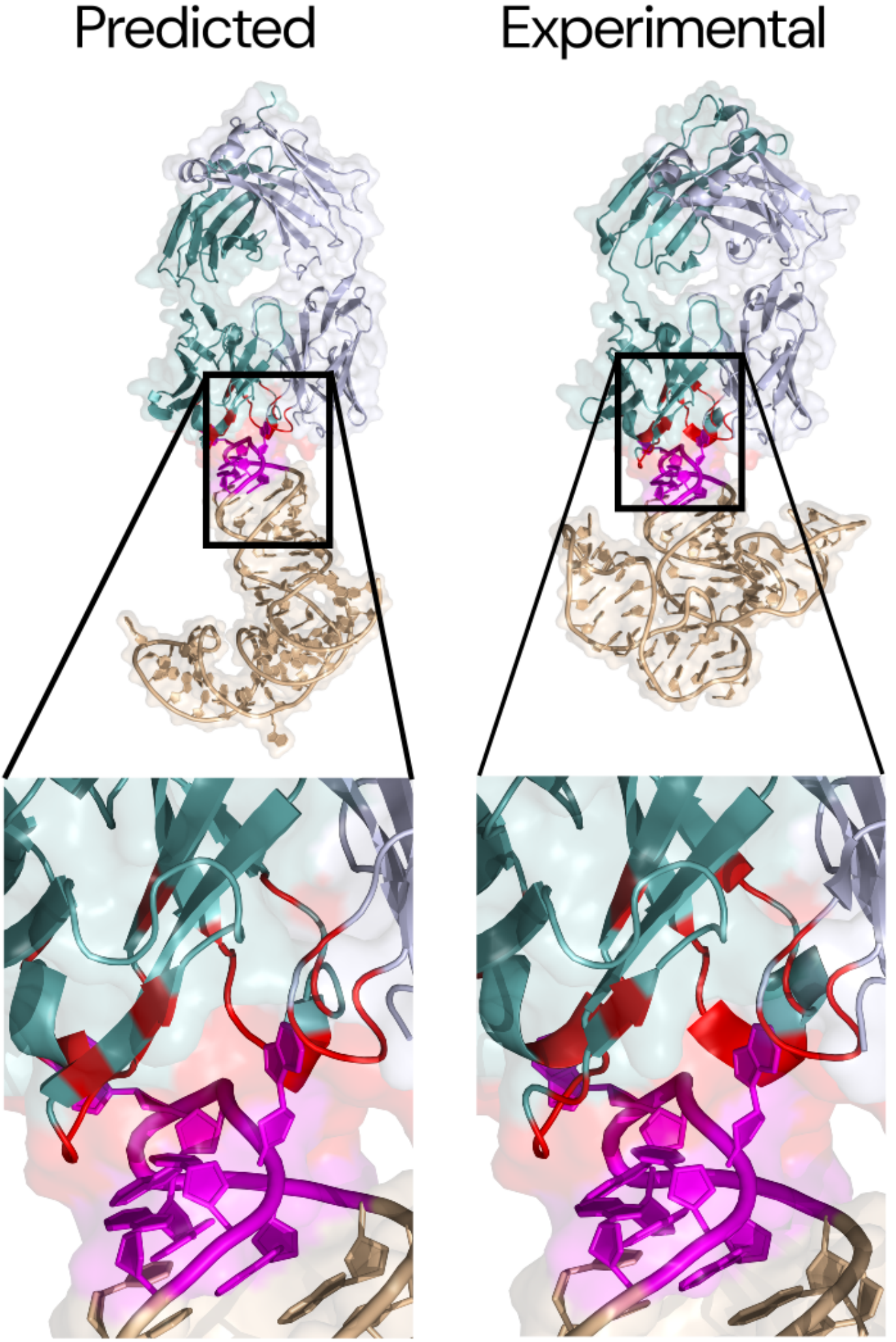
Predicted
Experimental

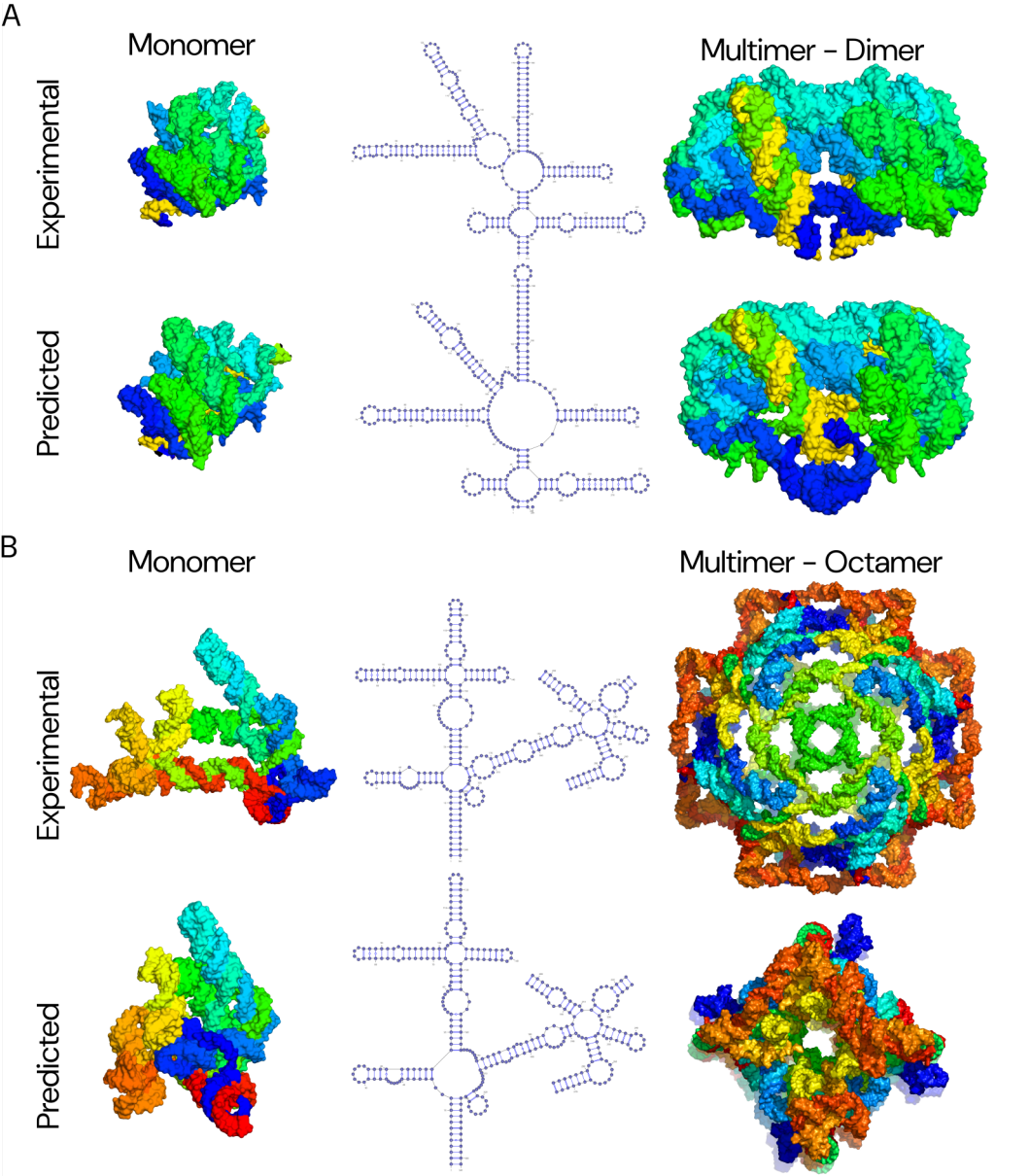
A
Monomer
Multimer – Dimer
Experimental
Predicted
B
Monomer
Multimer – Octamer
Experimental
Predicted